Polyelectrolyte Complex Hollow Fiber Membranes Prepared via Aqueous Phase Separation

ACS APPLIED POLYMER MATERIALS

pubs.acs.org/acsapm Article

Polyelectrolyte Complex Hollow Fiber Membranes Prepared via Aqueous Phase Separation

Muhammad Irshad Baig, Mehdi Pejman, Joshua D. Willott, Alberto Tiraferri, and Wiebe M. de Vos*

Cite This: https://doi.org/10.1021/acsapm.1c01464 Read Online

ACCESS | Metrics & More | Article Recommendations | Supporting Information

ABSTRACT: Hollow fiber (HF) membrane geometry is the preferred choice for most commercial membrane operations. Such fibers are conventionally prepared via the non-solvent-induced phase separation technique, which heavily relies on hazardous and reprotoxic organic solvents such as *N*-methyl pyrrolidone. A more sustainable alternative, i.e., aqueous phase separation (APS), was introduced recently that utilizes water as a solvent and non-solvent for the production of polymeric membranes. Herein, for the first time, we demonstrate the preparation of sustainable and functional HF membranes via the APS technique in a dry-jet wet spinning process. The dope solution comprising poly(sodium 4-styrenesulfonate) (PSS) and polyethyleneimine (PEI) at high pH along with an aqueous bore liquid is pushed through a single orifice spinneret into a low pH acetate buffer coagulation bath. Here, PEI becomes charged resulting in the formation of a polyelectrolyte complex with PSS. The compositions of the bore liquid and coagulation bath were systematically varied to study their effect on the structure and performance of the HF membranes. The microfiltration-type membranes (permeability ~500 to 800 $L \cdot m^{-2} \cdot h^{-1} \cdot bar^{-1}$) with complete retention of emulsion droplets were obtained when the precipitation rate was slow. Increasing the concentration of the acetate buffer in the bath led to the increase in precipitation rate resulting in ultrafiltration-type membranes (permeability ~12 to 15 $L \cdot m^{-2} \cdot h^{-1} \cdot bar^{-1}$) having molecular weight cut-offs in the range of ~7.8−11.6 kDa. The research presented in this work confirms the versatility of APS and moves it another step closer to large-scale use.

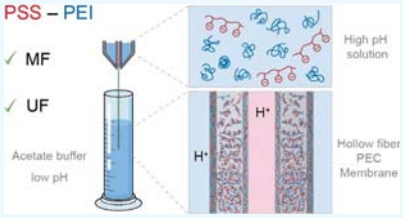

KEYWORDS: *sustainable, hollow fiber, membranes, aqueous phase separation, polyelectrolyte complex*

1. INTRODUCTION

Hollow fiber membranes are the result of decades of dedicated research and development on reverse osmosis membranes, initiated by industrial giants such as Mahon, Dow, and Du Pont in the 1960s.[1] Since then, hollow fibers have been used for many applications; from the medical field[2,3] to water purification[4−7] and gas separation.[8,9] There are clear advantages to using the hollow fiber membrane geometry as compared to the flat sheet and tubular geometries, including their higher per unit volume productivity resulting from the high packing density.[1] To better illustrate this point, as an example, a 0.04 m^3 membrane vessel can house 575 m^2 of the 90 μm-diameter hollow fibers and only 30 m^2 of the spiral-wound flat sheet membranes.[10] In addition, hollow fibers can be potted and hosted for mass packing, as opposed to the spiral-wound and tubular configurations that require additional hardware such as spacers and/or porous supports.

Currently, hollow fiber polymeric membranes are fabricated via a procedure known as non-solvent-induced phase separation (NIPS), which was first developed by Loeb and Sourirajan to produce flat sheet membranes for seawater demineralization.[11] To obtain the hollow fiber membranes via NIPS, the polymer is first dissolved in an organic solvent, such as *N*-methyl pyrrolidone (NMP), and subsequently extruded through a spinneret into a non-solvent coagulation bath, typically water. The polymer, being insoluble in the non-solvent bath, precipitates as a solid porous film.[12] Two coagulants are involved in the hollow fiber membrane production process: an internal coagulant that determines the membrane morphology at the inner (lumen) side and an external coagulant that affects the morphology of the outer surface of the membranes. As a result, the location and properties of the selective skin layer can be influenced by carefully choosing the internal and external coagulants. In addition, the choice of polymer, solvent, and non-solvent is critically important to control the resulting membrane pore structure and morphology.[13,14] Such control over the membrane structure has made NIPS a versatile technique that is dominant in the production of polymeric membranes for all separation processes.

One of the major problems with NIPS is the excessive use of toxic solvents such as the reprotoxic NMP. The toxicity of NMP can adversely affect human health and also imposes massive recycling costs to satisfy the stringent environmental regulations. Due to these reasons, the use of NMP has been

Received: October 26, 2021
Accepted: December 29, 2021

restricted by the European Union through Registration, Evaluation, Authorisation and Restriction of Chemicals (REACH) legislation.[15]

A more sustainable alternative is to utilize water as a solvent, although its potential remains largely untapped as most polymers used for NIPS are simply not water-soluble. Enter polyelectrolytes (PE), a class of polymers that are soluble in water with a negative or positive charge on their repeating units, surrounded by counter-ions. Upon interaction of two oppositely charged PEs, a gain in entropy due to the release of the bound counter-ions leads to the formation of polyelectrolyte complexes (PEC), which can themselves be water-insoluble solid materials.[16,17] Schaaf and Schlenoff have demonstrated that PECs can be processed and used in a multitude of applications including biocomposites, self-healing materials, and synthetic cartilage.[18] Additionally, PECs have been prominently used in drug delivery and gene therapy applications mainly due to their stimuli-responsive behavior.[19] Decher and Hong utilized the oppositely charged PE to build ultrathin multilayers by means of a self-assembly process.[20] After this, many studies were carried out to produce multilayer coating of PE on a porous membrane support.[21−24] Such polyelectrolyte multilayer membranes are widely utilized for nanofiltration applications where the removal of salt and/or small organic molecules (150 Da to 1000 Da) is desired.

Recently, our group has utilized PE to fabricate free-standing PEC membranes in a completely aqueous approach by regulating either the pH or salinity as a phase separation trigger,[25−28] thus eliminating the need for NMP. In this approach, known as aqueous phase separation (APS), water acts as both the solvent and the non-solvent according to the pH/salinity conditions. This tunability of the phase separation kinetics, similar to NIPS, gives a great deal of control over the final pore structure of the membranes and leads to a range of porous and dense membranes with suitable separation performance. In our previous works, we discussed the effects of the change in salinity, pH, and the crosslinking conditions on the process of PE membrane preparation.[26,29,30] The combination of poly(sodium 4-styrenesulfonate) (PSS) as the polyanion with polyethyleneimine (PEI) as the polycation was especially promising because it operates under mild pH conditions and forms both micro- and ultrafiltration-type membranes having higher pure water permeabilities and good separation properties. These two PE have versatile properties and have been used in a variety of applications such as a cathode interfacial layer for electron extraction,[31] micro/nano-patterned structures for optical sensors,[32] and coating materials for multilayer membranes.[33,34]

In the PSS−PEI system, the phase separation is triggered by changing the pH conditions as explored in our previous work.[29] A mixture of PSS and PEI in reported ratios yielded a solution with a pH of 12 (no base added), where PEI is uncharged. Exposing this solution to an acidic environment having a pH of 4, where PEI becomes fully charged, results in the formation of a porous water-insoluble polyelectrolyte complex with PSS. As the change in pH conditions is the driving force for phase separation, it can be regulated to control the rate of precipitation. It was found that reducing the pH generally brought about a faster onset of precipitation and a faster precipitation rate. Similar effects were observed upon increasing the buffer concentration under stable pH conditions.[29] These two parameters provide a great set of tools to fine-tune the morphology and the pore structure of the resulting PSS−PEI membranes.

So far, nearly all APS studies have focused on producing flat sheet membranes, including the relatively successful PSS−PEI system. Recently, Emonds et al. fabricated the tubular PEC membranes using PSS and poly(diallyldimethylammonium chloride) (PDADMAC) exploiting salinity as the stimulus for phase separation.[35] Their work provided a significant breakthrough in material engineering toward smaller tubular geometries. However, preparing a stable hollow fiber membrane still remains a significant challenge. Indeed, concentrating attempts toward the hollow fiber PEC membrane fabrication is the natural next step in solvent-free membrane production via APS for large-scale applications.

In this study, we prepare the PSS−PEI-based hollow fiber membranes via the APS method. To our knowledge, this is the first report on the polyelectrolyte complex-based hollow fiber membranes. PSS and PEI were mixed without any additives to obtain a homogeneous solution that can be precipitated as a functional membrane in a mild-pH acetate buffer (pH 3.6−5).[29] The hollow fibers are spun in a dry-jet wet spinning fashion. During spinning, the characteristics of the lumen (or inner) side are primarily determined by the bore fluid composition, whereas the outer skin of the fiber is mostly determined by the coagulation bath composition. In addition, the acetate buffer bath pH and concentration and the bore fluid composition are explored to gain control over the final fiber structure. The scanning electron microscopy (SEM) micrographs of the fibers highlight how the different tuning parameters control the fiber shape and morphology. Pure water permeability (PWP) and retention tests were used to evaluate the performance and membrane type of the hollow fiber membranes. This study confirms the feasibility of APS-based hollow fiber membrane preparation, opening the field of sustainable APS hollow fiber membrane production.

2. EXPERIMENTAL SECTION

2.1. Materials. Poly(sodium 4-styrene sulfonate) (PSS, powder form, M_w ∼1000 kDa), branched polyethyleneimine (PEI) (>99%, M_w ∼25 kDa), sodium acetate anhydrous (reagent plus, 99%), glacial acetic acid (ACS reagent, ≥99%), glutaraldehyde (GA, 50 wt % in water), glycerol (ACS reagent, ≥99.5%), *n*-hexadecane (>99%), sodium dodecyl sulfate (SDS, >99%), Oil red EGN (solvent red 26, analytical standard), polyethylene glycol (PEG) with molecular weights of 1500, 3000, 6000, 10,000, 20,000, and 35,000 Da, albumin from bovine serum (BSA) as lyophilized powder (≥98%), sodium phosphate dibasic heptahydrate (>99.9%), and sodium phosphate monobasic dihydrate (>99%) were purchased from Merck, The Netherlands. A Milli-Q Ultrapure water purification system was used to obtain the deionized water. All the chemicals were used without any further purification.

2.2. Preparation of the Dope Solution. First, a 35 wt % aqueous solution of PSS was prepared by dissolving the pure PSS in deionized water. Similarly, deionized water was added to PEI to obtain a 35 wt % aqueous solution. The two polyelectrolyte solutions were then mixed in a monomer molar mixing ratio of 1:2 of PSS:PEI to obtain a 35 wt % dope solution, which was stirred until it became homogeneous. The molar mixing ratio was calculated based on the molecular weights of the monomers of PSS (∼206 Da) and PEI (∼43 Da, per ethyleneimine unit). The composition of the dope solution is shown in Table 1. The pH of the dope solution was ∼12 as measured using a calibrated handheld pH meter (pH 110, VWR).

The viscosity of the dope solution was measured on a HAAKE Viscotester 550 Rotational Viscometer (ThermoFisher Scientific, USA). Approximately 25 mL dope solution was poured into the SV-DIN spindle cylinder, which was then mounted on the viscometer.

https://doi.org/10.1021/acsapm.1c01464
ACS Appl. Polym. Mater. XXXX, XXX, XXX−XXX

Table 1. Composition of the PSS−PEI Dope Solution

Dope solution	PSS (wt %)	PEI (wt %)	Water (wt %)
PSS:PEI (1:2)	24.7	10.3	65

The dynamic viscosity of the dope solution was measured at 20 °C from low to a high shear rate (24.9 s^{-1} to 1000 s^{-1}). The dope solution had a dynamic viscosity of ∼2.5 ± 0.2 Pa·s at a shear rate of 24.9 s^{-1}.

2.3. Hollow Fiber Membrane Spinning. The PSS−PEI hollow fiber membranes were spun at room temperature using the dry-jet wet spinning method. The dope solution was first poured into a stainless steel syringe (Chemyx Inc., USA) and left to de-gas overnight. The acetate buffer baths used to precipitate the PSS−PEI dope solution were prepared by mixing acetic acid and sodium acetate in specific amounts. Five pH 4 buffer baths were prepared at varying concentrations of 0.1, 0.25, 0.4, 0.5, and 0.75 M. For the 0.5 M buffer bath, the pH was varied from 3.6, 4, 4.5, and 5 by changing the ratio of acetic acid and sodium acetate while keeping the overall buffer concentration constant. In addition, 0.01 wt % glutaraldehyde (GA) was added to all the coagulation baths as a crosslinking agent, which reacts with the amine groups of PEI to form the imine bonds via the Schiff base reaction.[36] This leads to the densification of the membrane as reported in our earlier works.[25,29] Four different types of bore liquids were investigated to produce the hollow fibers: (i) deionized water; (ii) an aqueous solution of glycerol (30 wt % and 50 wt %); (iii) 0.25 M acetate buffer at pH 4; and (iv) a mixture of 0.25 M acetate buffer at pH 4 with 30 wt % glycerol.

Given that the pH of the PSS−PEI dope solution is approximately ∼12, it is necessary to have a spinneret that can withstand the high pH and high salinity. Therefore, a special single-orifice spinneret with no welded parts was used for the production of the hollow fiber membranes. The diameter of the spinneret needle was 1 mm with a cap having a diameter of 1.6 mm. The flow rates of the dope solution and the bore liquid were kept constant at 3 mL·min^{-1}, and the air gap length was kept at ∼11 cm for all the membranes. First, the bore liquid was pumped through the spinneret needle followed by the dope solution. The resultant fiber was allowed to fall in the coagulation bath under the action of gravity as shown in Figure 1. The fibers were not drawn (or pulled) through the coagulation bath, meaning that there was no take-up velocity. The fibers were kept in the coagulation bath for 18 h, which is also the crosslinking time. After this time, they were removed from the bath, thoroughly washed, and stored in deionized water for further use.

2.4. Membrane Characterization. The surface and cross-section morphologies of the hollow fiber membranes were observed with scanning electron microscopy, SEM (JSM-6010LA, JEOL, Japan). All the membrane samples for SEM were first stored in a 20 wt % glycerol solution for 4 h, before being taken out, and left to dry inside an aerated fume hood. For the cross-section SEM imaging, the dried hollow fiber membranes were immersed in liquid N_2 for 20 s and carefully fractured to reveal the cross-section. The SEM samples were then stored in a vacuum oven operating at 30 °C for 24 h. Before taking the SEM images, the samples were sputter coated with a 5 nm thin layer of the Pt/Pd alloy using a Quorum Q150T ES (Quorum Technologies, Ltd., UK) sputter coater. Atomic force microscopy (AFM) was conducted in non-contact tapping mode in air using Dimension Icon, Bruker. An area of 2 μm by 2 μm was scanned, and the average roughness was measured via the built-in software. Water contact angle measurements were conducted on the outer side of the fiber by the sessile drop technique using a contact angle analyzer (OCA 20, DataPhysics Instruments GmbH, Germany) at 20 °C. The surface of the membrane was wetted with a 2 μL water droplet, and the angle was measured after 5 s using a built-in software.

For the PWP measurements, the hollow fiber membranes were first potted into modules with one fiber each and an effective membrane length of 6.5 cm. For each different type of membrane, three modules were prepared, and the average value with standard deviation is reported. The PWP was measured in a dead-end configuration with a shell (outer) side feed, see Figure S1 of the Supporting Information. The permeability tests were conducted at an applied water pressure of 1 bar, and the mass of the permeating water was measured automatically on a weighing balance connected to a computer. The PWP (P, in L·m^{-2}·h^{-1}·bar^{-1}) was calculated using eq 1

$$P = \frac{J_W}{\Delta p} \tag{1}$$

Here, J_W is the pure water flux calculated from the change in permeate volume (L) per unit effective membrane area (3.26 cm^2) per unit time

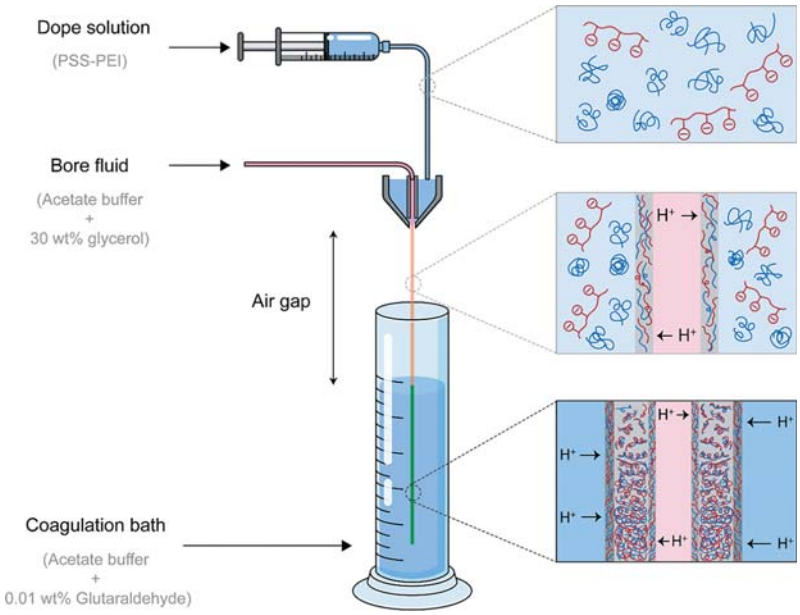

Figure 1. Schematic illustration of the dry-jet wet spinning process to produce the PSS−PEI hollow fiber membranes via the APS technique. The dope solution contains the strong polyanion, PSS, in its charged state and PEI in its uncharged state. The dope solution is pushed through the single-orifice spinneret and is immersed in the acetate buffer coagulation bath.

https://doi.org/10.1021/acsapm.1c01464
ACS Appl. Polym. Mater. XXXX, XXX, XXX−XXX

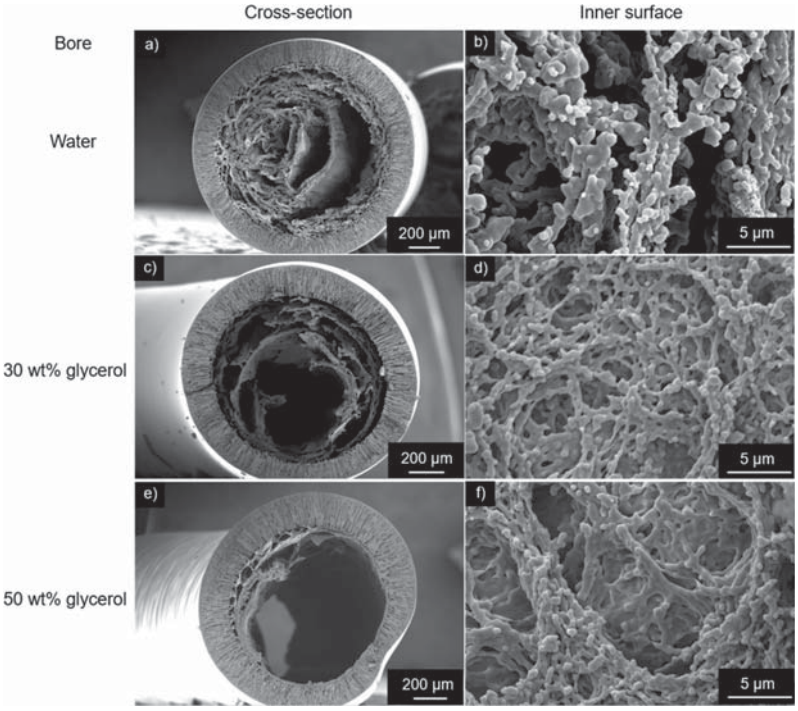

Figure 2. Cross-section and the inner (lumen side) surface SEM images of the PSS−PEI hollow fiber membranes showing the effect of adding glycerol in the bore liquid. (a−b) Only water, (c−d) 30 wt % glycerol, and (e−f) 50 wt % glycerol as the bore liquid. The membranes were prepared in coagulation baths containing 0.5 M acetate buffer at pH 4 with 0.01 wt % glutaraldehyde.

(h), and Δp is the pressure difference (bar) between the feed and the permeate side.

The microfiltration performance of the membranes was evaluated using an oil-in-water emulsion that was prepared following the procedure described by Dickhout et al.[37] Briefly, 100 mg·L^{-1} *n*-hexadecane containing 20 mg·L^{-1} Oil red EGN (dye) was added to 463 mg·L^{-1} SDS while stirring at 14,000 rpm for 20 min. The average diameter of the oil droplet in the emulsion was 3−4 μm.[37] Oil red EGN is only soluble in *n*-hexadecane and, therefore, is used as a marker for the oil droplets. The *n*-hexadecane oil droplet retention tests were conducted at 0.4 bar of feed pressure in the dead-end configuration. The feed and permeate samples were analyzed via a UV−vis spectrophotometer (Shimadzu UV-1800, Japan) at λ_{max} = 521 nm, which corresponds to the maximum absorbance wavelength of the dye. A calibration curve was obtained with known concentrations of the *n*-hexadecane in the SDS emulsion. This calibration curve was linear, which means that the absorbance data could be directly correlated to the concentration of *n*-hexadecane in the sample. The retention (R) was then calculated using eq 2

$$R = \left[1 - \frac{C_p}{C_f}\right] \times 100 \quad (2)$$

where C_p and C_f are the concentrations of *n*-hexadecane in the permeate and in the feed side, respectively.

For the molecular weight cut-off (MWCO) measurements, an aqueous solution of PEGs having different molecular weights, i.e., 1500, 3000, 6000, 10,000, 20,000, and 35,000 Da, was used. This solution was prepared by dissolving 1 g·L^{-1} of each individual PEG in deionized water. The PEG solution was filtered through the membranes in a dead-end configuration with the feed from the shell side. The feed and the permeate streams were collected and analyzed via gel permeation chromatography (GPC, Agilent 1200/1260 Infinity GPC/SEC series, Polymer Standards Service data center and column compartment). Milli-Q ultrapure water containing 50 mg·L^{-1} NaN_3 was used as the eluent at a flow rate of 1 mL·min^{-1} through the GPC column (10 μm Polymer Standards Service Suprema 8 × 300 mm 1000 Å and 10 μm 30 Å, connected in series). The concentration of the PEGs in the feed and permeate streams was determined, and the retention rate was then calculated using eq 2. MWCO was estimated by constructing a sieving curve of retention (%) as a function of the molecular weight of PEG (Da). The molecular weight of PEG that corresponds to 90% retention is the MWCO of the membrane.

The ultrafiltration performance of the hollow fiber membranes was analyzed similarly by filtering an aqueous solution of BSA through the membranes in a dead-end configuration at 1 bar of pressure with a shell-side feed. The solution was prepared by dissolving 0.1 wt % BSA in 0.1 M phosphate buffer at pH 7.4. The pH was adjusted using 0.1 M HCl/NaOH solution. The phosphate buffer consisted of sodium phosphate dibasic heptahydrate and sodium phosphate monobasic dihydrate. The feed and permeate samples were collected and analyzed via UV−vis spectrophotometry at λ_{max} = 280 nm, which is the maximum absorbance wavelength of BSA. The BSA retention was calculated using eq 2.

3. RESULTS AND DISCUSSION

3.1. Effect of Composition of the Bore Liquid. In comparison to the flat sheet membranes, the hollow fiber membrane geometry provides additional parameters to control the rate of precipitation and the resulting membrane morphology. One such parameter is the composition of the bore liquid, which influences the structure of the lumen or inner side of the hollow fibers.[38,39] The bore liquid composition was carefully selected after several preliminary trials to obtain the mechanically strong membranes. As for the coagulation bath, we take inspiration from our earlier work on the PSS−PEI flat sheet membranes[29] and select 0.5 M acetate buffer at pH 4, which is a strong non-solvent for PSS−PEI providing a dense skin layer.

In the first experiments, deionized water was used as the bore liquid, and this resulted in the membranes without the desired hollow structure, see Figure 2a. Water at near neutral pH values does not trigger the polyelectrolyte complexation

https://doi.org/10.1021/acsapm.1c01464
ACS Appl. Polym. Mater. XXXX, XXX, XXX−XXX

between PSS and PEI, and as a result, the direction of precipitation is from the outside of the fiber (acetate buffer bath) toward the inner lumen side (bore side, water). Furthermore, the combination of viscosity and flow rate of the water (bore liquid in this case) was not sufficient to maintain the hollow structure at the lumen side. In an attempt to improve the structural integrity of the fibers, the bore liquid flow rate was first increased from 3 mL·min^{-1} to 5 mL·min^{-1} and then to 6 mL·min^{-1}. However, this approach was unsuccessful and resulted in fibers with thinner walls causing them to fracture easily. Although these initial measurements did not immediately lead to the ideal HF membranes, they do already provide clear indications that the HF geometry is possible with the APS approach, but further tuning is required.

Another approach to improve the hollow shape of the fibers was to increase the viscosity of the bore liquid. It is known from previous reports that adding glycerol increases the viscosity of the bore liquid and can prevent the hollow fiber membranes from collapsing[40] Therefore, aqueous solutions of 30 wt % and 50 wt % glycerol were used as the bore liquids. The impact of the added glycerol can clearly be observed in the representative cross-section SEM images shown in Figure 2c,e, where the resultant membranes present the suitable hollow lumen contours. However, these membranes lacked the mechanical strength to sustain 1 bar of feed water pressure. This structural instability is attributed to the fact that no precipitation occurred at the lumen side because the combination of water and glycerol is also not a non-solvent for PSS−PEI. Here, the sole direction of precipitation is from the outside of the fiber (acetate buffer) toward the lumen side, and as a result, the lumen surfaces are porous with uneven porosity as shown in Figure 2d,f. Although the addition of glycerol in the bore liquid helps maintain the hollow structure of the lumen side, this protocol does not provide adequate mechanical stability for the hollow fibers to withstand the applied water pressures.

Conversely, the hollow fiber membranes prepared using a strong non-solvent, i.e., the acetate buffer in the bore liquid, resulted in membranes with skin layers on both the lumen and the outer surfaces as shown in the cross-section SEM images of Figure S2a,c,e. However, the inner diameter of the membranes was not consistent along the fiber length, thus resulting in the irregular lumen side contours. This observation is most obvious when 0.75 M acetate buffer was used as the bore liquid, where the resultant membranes had an oval-shaped lumen structure. Peng et al. concluded that such a contour in the hollow fiber is due to the significantly faster precipitation rates on the lumen side and can be overcome by reducing the rate of precipitation.[41] It is known from our previous work on the PSS−PEI flat sheet membranes that the rate of precipitation increases with the increases in buffer concentration.[29] Here, the buffer capacity increases at higher acetate concentrations, thereby lowering the pH of the PSS−PEI dope solution relatively quicker. As the pH gradient is the driving force for this version of APS, a faster change in solution pH that occurs at higher buffer concentrations results in a more rapid polyelectrolyte complexation of PSS and PEI. Therefore, due to the slower precipitation rate of the membranes prepared in 0.25 and 0.5 M acetate buffer, the oval-shaped contour of the hollow fiber does not exist in these membranes. Using a strong non-solvent in the bore means that the dope solution precipitates as soon as it comes in contact with the bore liquid and continues precipitating from the inside throughout the entire length of the air gap (∼11 cm in this case, see Figure 1). A dense skin layer is immediately formed on the lumen side of the fiber due to the instantaneous precipitation induced by the acetate buffer, and this skin layer acts as a barrier for further mass transfer. As a result, an asymmetric structure with a dense skin and a porous substructure is formed on the lumen side. Then, as soon as the dope solution comes in contact with the coagulation bath, the precipitation process also begins from the outer surface and continues toward inside. Here, a dense skin layer with a porous substructure is also formed at the outer surface of the fiber. These two dense skin layers on both sides of the fiber act as barriers for the solvent (high pH) and non-solvent (low pH buffer) exchange resulting in an asymmetric membrane morphology.[42] As a result, a three-layered structure is formed where a highly porous layer is sandwiched between the two relatively dense layers, and this ultimately leads to delamination; see the cross-section images in Figure S2a,c,e in the Supporting Information. In addition, the rapid rate of precipitation on the lumen side eventually leads to hollow fibers having irregular contours and could not be further processed.

It has now been established that using glycerol as the bore liquid results in the membranes having only the outer skin layer and a completely porous lumen side (Figure 2), whereas using acetate buffer as the bore liquid results in the membranes having two skin layers with a porous structure sandwiched in between (Figure S2). Therefore, a combination of these two bore liquids should be beneficial in controlling the structure of the hollow fiber membrane so as to obtain an outer skin layer with a relatively less porous lumen side. As the acetate buffer is a strong non-solvent for PSS−PEI and facilitates rapid precipitation, the addition of glycerol to the bore liquid increases its viscosity and slows down the rate of precipitation. Thus, the concentration of glycerol and the acetate buffer can be carefully tuned to obtain the desired membrane structures on the lumen side of the fiber. In this case, the concentration of glycerol was fixed at 30 wt %, and the concentration of the pH 4 acetate buffer was varied from 0.25 to 0.75 M, see Figure S3 in the Supporting Information. When the bore liquid containing 0.25 M acetate buffer with 30 wt % glycerol was used, the resultant hollow fiber membranes showed a porous lumen surface (Figure S3b) because of the slower rate of precipitation. As the acetate buffer concentration in the glycerol containing the bore liquid was increased to 0.5 M and then further to 0.75 M, the resultant hollow fiber membranes had increasingly dense skin layers on the lumen side of the fiber, see Figure S3d and f . These membranes with two skin layers (inner and outer) were mechanically weak and could not withstand water pressure. Consequently, the most suitable bore liquid for the system investigated in this study consisted of 0.25 M acetate buffer with 30 wt % glycerol. This solution resulted in a dense outer layer and a more porous and hollow lumen side and was thus chosen to produce the hollow fiber membranes and investigate the effect of additional parameters on their structure and performance.

3.2. Effect of Acetate Buffer Concentration in the Coagulation Bath. Now that the composition of the bore liquid was fixed, the concentration of acetate buffer in the coagulation bath was investigated. Figure 3 shows the cross-section SEM images of the PSS−PEI hollow fiber membranes prepared using different concentrations of pH 4 acetate buffer in the coagulation bath.

https://doi.org/10.1021/acsapm.1c01464
ACS Appl. Polym. Mater. XXXX, XXX, XXX−XXX

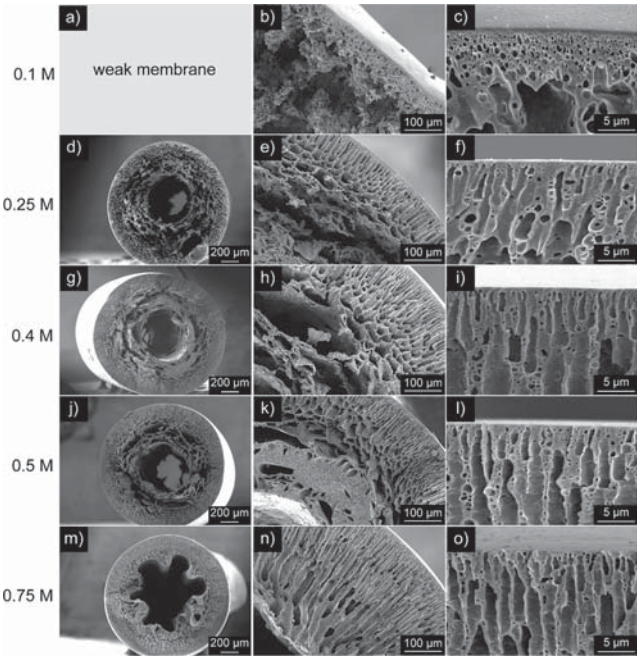

Figure 3. Cross-section SEM images of the PSS−PEI hollow fiber membranes showing the effect of acetate buffer concentration in the coagulation bath on the membrane morphology. (a−c) 0.1, (d−f) 0.25, (g−i) 0.4, (j−l) 0.5, and (m−o) 0.75 M acetate buffer concentrations in the coagulation bath.

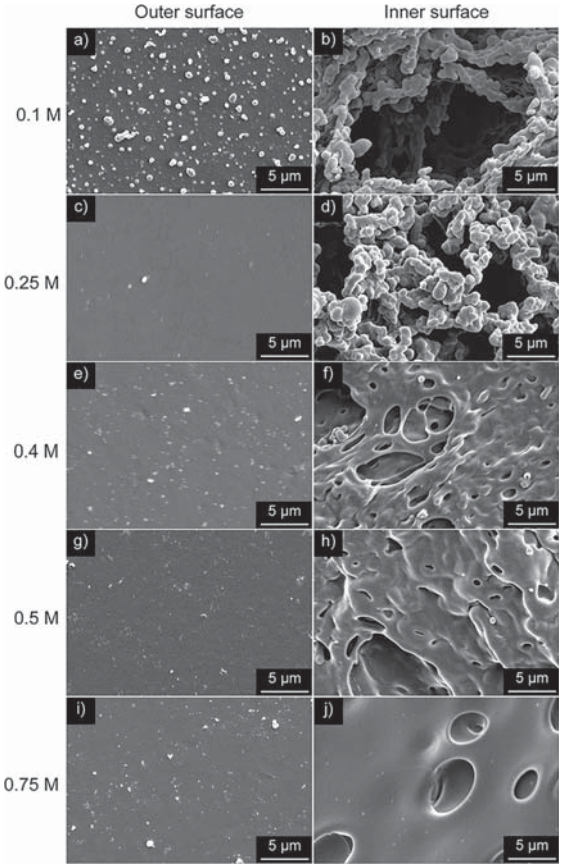

Figure 4. SEM images of the outer and inner (lumen) surfaces of the PSS−PEI hollow fiber membranes prepared in different concentrations of pH 4 acetate buffer. (a−b) 0.1, (c−d) 0.25, (e−f) 0.4, (g−h) 0.5, and (i−j) 0.75 M.

As described earlier, the rate of precipitation increases with the increase in the acetate buffer concentration. The rate of precipitation was slow (>10 min) for the membranes prepared in 0.1 M acetate buffer. In this case, the amount of acetate buffer was not sufficient to sustain the solvent (high pH) and non-solvent (acetate buffer) exchange throughout the thickness of the fiber. As a result, a small region close to the coagulation bath precipitated first, whereas the rest precipitated at a relatively slower rate. This phenomenon can be observed by looking at the cross-section SEM image in Figure 3b where the region closer to the coagulation bath, i.e., the outer surface of the fiber, has an asymmetric structure with the finger-like macrovoids. The thickness of this region is approximately ∼100 μm. A higher magnification image of this region is shown in Figure 3c where the relatively denser outer most skin layer with more oval-shaped macrovoids in the immediate substructure can be clearly observed. After formation of the outer skin, the rate of precipitation was significantly slowed down, and the concentration of the buffer was not sufficient to continue the precipitation at the same rate. This mechanism resulted in a more open substructure as observed in the SEM image of the lumen surface shown in Figure 4b. The images also indicate extreme delamination of the membrane due to their mechanical fragility.

Increasing the acetate buffer concentration to 0.25 M resulted in the fibers precipitating instantaneously (<1 s). The effects of instantaneous precipitation are immediately visible in the SEM image of Figure 3f, which reveals a typical asymmetric structure with a dense top layer (shown in Figure 4c) and the finger-like macrovoids in the substructure. This kind of asymmetric structure is typically associated with the instantaneous phase separation in NIPS.[42,43] In addition, the lumen surface of these membranes was less porous (Figure 4d) as compared to the fibers prepared in 0.1 M acetate buffer bath (Figure 4b).

Further increasing the acetate buffer concentration to 0.4 M and then to 0.5 M increased the rate of precipitation through the thickness of the fiber, which resulted in the membranes with elongated finger-like macrovoids as seen in Figure 3i,l. Both these membranes had dense layers on the outer side of the fiber (Figure 4e,g). Furthermore, the lumen (inner) surfaces of these membranes were significantly more compact than those obtained in 0.1 M and 0.25 M acetate buffer (compare Figure 4d,f,h). Further increasing the acetate buffer concentration to 0.75 M resulted in the hollow fiber membranes with irregular lumen structures and finger-like macrovoids throughout the thickness of the fiber (Figure 3n). Santoso et al. attributed such an irregular lumen contour to the rapid formation of a dense skin layer on the inner side of the fiber that causes stresses and strains on the developing fiber.[44] These types of hollow fiber contours are undesired because they negatively influence the mechanical strength and also the performance of the membranes. The lumen surface of this membrane also had a denser structure compared to the rest of the fibers, see Figure 4j.

The pure water permeability values at 1 bar of applied water pressure were measured for the hollow fiber membranes, and the results are presented in Figure 5. The hollow fiber membranes prepared in the 0.25 M acetate buffer bath concentration ruptured under the applied water pressure because of their porous structure and weaker mechanical

https://doi.org/10.1021/acsapm.1c01464
ACS Appl. Polym. Mater. XXXX, XXX, XXX−XXX

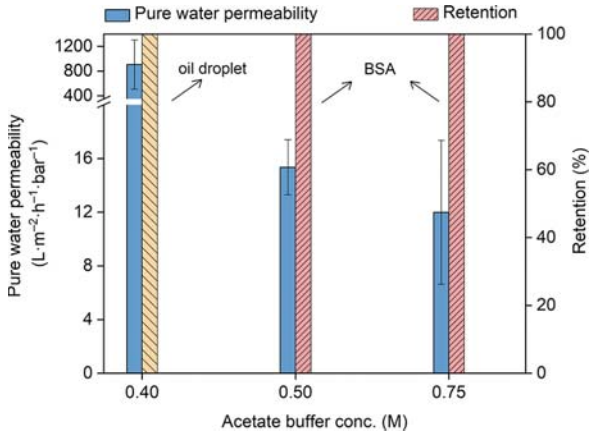

Figure 5. Effect of acetate buffer concentration in the coagulation bath on the pure water permeability and *n*-hexadecane oil droplet/BSA retention of the PSS−PEI hollow fiber membranes. The membranes were prepared in pH 4 acetate buffer containing 0.01 wt % GA.

strength. The membranes prepared in 0.4 M buffer had a high pure water permeability (PWP) of ∼900 ± 400 $L{\cdot}m^{-2}{\cdot}h^{-1}{\cdot}bar^{-1}$ even though no pores on the top surface of the membranes were visible at magnifications of up to ×10,000, see Figure 4e. Such a high permeability may possibly be due to the formation of the small cracks during membrane operation. Nevertheless, the membranes showed a stable PWP, and therefore, their retention performance was also measured. An oil-in-water emulsion having an oil-droplet size of 3−4 μm was filtered through the membrane at 0.4 bar of feed pressure. It was found that these membranes retained the oil-droplets with 100% retention. On the other hand, the membranes did not retain any protein (BSA), thus suggesting their potential use as microfiltration membranes.

In contrast, the membranes prepared in 0.5 and 0.75 M acetate buffer baths showed PWP of ∼15 ± 2 and 12 ± 5 $L{\cdot}m^{-2}{\cdot}h^{-1}{\cdot}bar^{-1}$, respectively. The larger error bar for the 0.75 M membranes could be attributed to its non-uniform lumen contour where the thickness of the fiber varies at different locations. The PWP values are more in accordance with the microstructure shown in Figure 4g,i where the top surface is dense and does not show any visible pores at the given magnification. The MWCO of these membranes, determined by the sieving curves shown in Figure S4, was ∼11,600 Da for the membranes prepared in 0.5 M and ∼7800 Da for the membranes prepared in 0.75 M acetate buffer. These values are typical for the ultrafiltration-type membranes where the MWCO can range from 1 to 1000 kDa.[45] For example, the MUF-10 K membrane by Toray Membrane USA Inc. has a MWCO of 10 kDa with a PWP of ∼23 $L{\cdot}m^{-2}{\cdot}h^{-1}{\cdot}bar^{-1}$.[46] Similarly, the polyethersulfone (PES) UF membrane by Microdyn−Nadir GmbH has a MWCO of 6 kDa with a PWP of ∼122 $L{\cdot}m^{-2}{\cdot}h^{-1}{\cdot}bar^{-1}$.[47] The membranes prepared in this work have comparable MWCO to the commercial membranes. However, future work needs to be devoted to increase the PWP of the PSS−PEI membranes.

The mean pore size of the membranes can be semi-quantitatively estimated by the MWCO (determined using PEG) of the membranes via the relation: $d = 0.09(M_w)^{0.44}$, first determined by Lentsch et al.[48] where d is in nm and M_w is in daltons (Da). Howe and Clark utilized this relation to accurately estimate the pore sizes of the ultrafiltration-type membranes.[49] Based on this equation, the estimated pore sizes of the 0.5 and 0.75 M membranes are ∼5.5 and 4.6 nm, respectively.

The membranes were also tested for protein retention using a 0.1 wt % BSA solution. BSA is a model protein solution used for evaluating the performance of the ultrafiltration type membranes as its molecular weight of ∼66 kDa and hydrodynamic radius of ∼4.3 nm are typical of many proteins.[50] The BSA solution was filtered through the membranes at a feed pressure of 1 bar, and the corresponding retention results are presented in Figure 5. It was found that the membranes prepared in 0.5 and 0.75 M acetate buffer completely retained BSA, in accordance with their estimated pore sizes.

The membrane prepared in 0.5 M acetate buffer was also tested for a longer period of time (∼7 days) under constant water pressure of 1 bar. The results shown in Figure S5a demonstrate that the membrane showed stable permeability for the entire duration of the test. This membrane had an

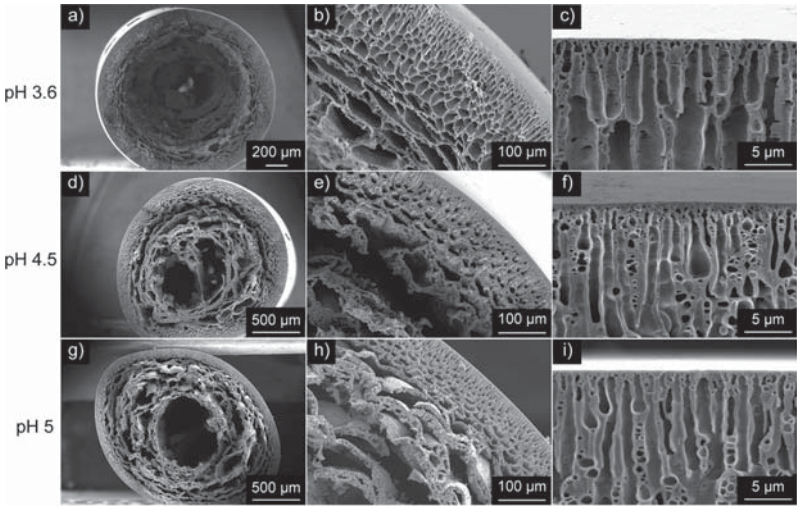

Figure 6. Cross-section SEM images showing the effect of pH of the acetate buffer in the coagulation bath on the membrane morphology. (a−c) pH 3.6, (d−f) pH 4.5, and (g−i) pH 5. The membranes were prepared in 0.5 M acetate buffer containing 0.01 wt % GA.

https://doi.org/10.1021/acsapm.1c01464
ACS Appl. Polym. Mater. XXXX, XXX, XXX−XXX

average surface roughness of ∼13 nm with an average water contact angle of ∼44°, Figure S6.

The results discussed above imply that the structure, morphology, and performance of the PSS−PEI hollow fiber membranes can be tuned by varying the spinning conditions. The concentration of the acetate buffer is one crucial parameter for this polyelectrolyte pair that determines the rate of precipitation both on the lumen and the shell side of the developing fibers. Both the micro- and tight ultrafiltration-type membranes were obtained by simply changing the concentration of the acetate buffer in the coagulation bath. In addition, the amount of glycerol and the acetate buffer added in the bore liquid can be controlled to adjust the precipitation on the lumen side. Another viable option to further control the precipitation kinetics in the lumen side might be to add a non-solvent, such as water at pH ∼8−10 in the bore liquid that would supposedly slow down the precipitation kinetics in the lumen side, thus resulting in a porous morphology. The tuning parameters available to control the precipitation kinetics and the resulting hollow fiber membrane morphology in APS are quite analogous to the traditional NIPS, whereby a multitude of the membrane structures can be produced simply by changing the spinning conditions.

3.3. Effect of the Coagulation Bath pH. In this version of APS, the polyelectrolyte complexation of PSS−PEI is induced by a pH shift. The dope solution has a pH of ∼12, in which PEI remains in its uncharged state. Lowering the pH of this solution to ∼4 (in the buffer bath) causes PEI to acquire charge and form a polyelectrolyte complex with the PSS. The commercially available branched PEI used in this work contains 31% primary, 39% secondary, and 30% tertiary amines[51] that have pK_a values of 4.5, 6.7, and 11.6,[52] respectively. As a result, varying the pH of the bath affects the charge density of PEI. The ionic crosslinking density and also the rate of precipitation can therefore be controlled by varying the pH of the coagulation bath, which is analogous to adding solvent to the non-solvent bath in the traditional NIPS.

The PSS−PEI hollow fiber membranes were prepared in 0.5 M acetate buffer at different values of the buffer pH, such as pH 3.6, pH 4, pH 4.5, and pH 5, to study the effect on the fiber structure and morphology. Figure 6 shows the cross-section SEM images of the resultant membranes. For the cross-section SEM images of the hollow fiber membranes prepared in pH 4, see Figure 3j,k,l.

Especially around the pK_a of 4.5, we expect that the pH will have a significant effect on the charge density of PEI, with the highest charge density at pH 3.6 and the lowest at pH 5. As a result, in pH 3.6, PSS and PEI likely form a highly crosslinked polyelectrolyte complex leading to instantaneous precipitation. This fast precipitation rate resulted in the asymmetric structures with a dense outer layer, shown in Figure 7a, and the finger-like macrovoids displayed in the SEM images of Figure 6b,c. The membranes also showed signs of delamination of the lumen side (Figure 6a), and hence, the inner surface SEM image presented in Figure 7b does not tell the complete story of these membranes. Furthermore, these membranes were rigid and fragile.

Increasing the buffer pH in the coagulation bath reduces the charge density of PEI leading to a reduced degree of ionic crosslinks. Furthermore, increasing the bath pH beyond the pK_a value of acetic acid (∼4.7) reduces the strength of the acid. As a result, the rate of precipitation is significantly slower for the membranes prepared at pH 5. Comparing the cross-section

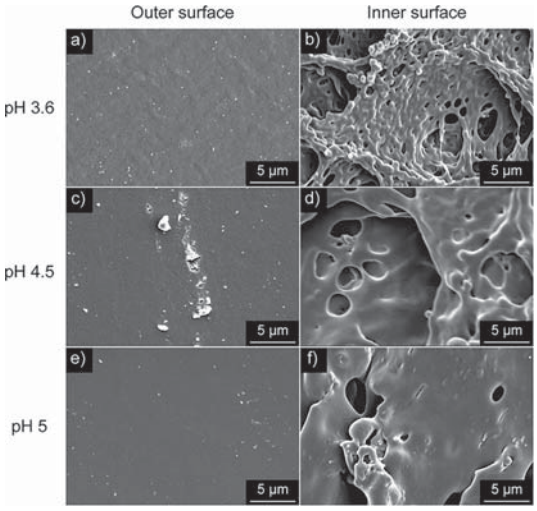

Figure 7. SEM images of the outer and inner (lumen) surfaces of the PSS−PEI hollow fiber membranes prepared in different pH values of 0.5 M acetate buffer. (a−b) pH 3.6, (c−d) pH 4.5, and (e−f) pH 5.

SEM images of Figure 6b,e,h (for these cases), it can be seen that the region around the outer surface of the fiber had finger-like macrovoids, and the size of the macrovoids decreased with increasing the bath pH. This observation is rationalized with the fact that the rate of PSS−PEI precipitation decreases at higher pH (>4.5), which in turn affects the formation of the macrovoids. Similar results are also obtained in the traditional NIPS where the rate of precipitation is slowed down upon the addition of solvent in the non-solvent bath.[53] The membranes prepared at pH 4.5 and 5 were also not circular, as seen in the SEM images of Figure 6d,g. The irregular outer surface might also possibly be due to the slower rate of precipitation, which may cause a degree of hydrodynamic instability in the dope solution during precipitation in the coagulation bath. Accordingly, the lumen side of these membranes was more porous as visible in Figure 6d,g.

The PWP of the membranes was measured at 1 bar of applied water pressure, and the results are shown in Figure 8. The PWP of membranes prepared in pH 3.6 was ∼540 ± 110 $L \cdot m^{-2} \cdot h^{-1} \cdot bar^{-1}$. As mentioned above, these membranes were

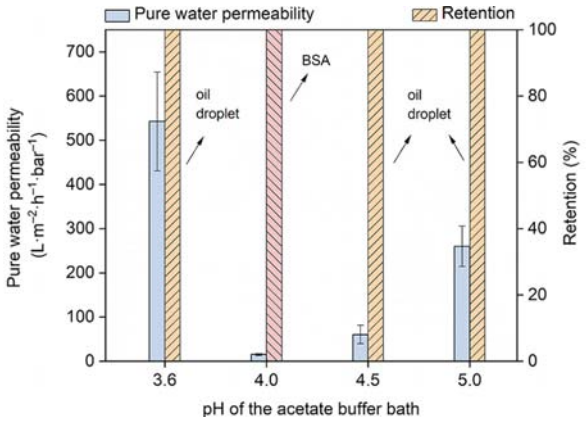

Figure 8. Effect of pH of the acetate buffer in the coagulation bath on the pure water permeability of the PSS−PEI hollow fiber membranes. The membranes were prepared in 0.5 M acetate buffer containing 0.01 wt % GA.

https://doi.org/10.1021/acsapm.1c01464
ACS Appl. Polym. Mater. XXXX, XXX, XXX−XXX

rigid and relatively fragile and therefore could possibly develop micro-cracks at applied water pressures. Consequently, the membranes displayed a high PWP with a large error bar while retaining 100% of the *n*-hexadecane oil droplets. However, they did not retain BSA, making them more suitable for microfiltration applications. In comparison, the membranes prepared at pH 4.5 and 5 showed PWPs of ∼60 ± 21 and 260 ± 46 $L{\cdot}m^{-2}{\cdot}h^{-1}{\cdot}bar^{-1}$, respectively, with a smaller error bar. Unfortunately, these membranes also did not show any retention for BSA, meaning that their pore size was larger than the size of BSA, i.e., ∼9 nm. These membranes also retained 100% oil droplets and may therefore also be more suited for the open ultrafiltration or microfiltration-type applications.

Overall, the presented APS hollow fiber membranes showed interesting properties and structures that can be fine-tuned by varying the pH of the acetate buffer. Therefore, the buffer bath pH may be used in combination with the buffer concentration to gain more control over the precipitation kinetics. For example, slightly lower acetate buffer concentrations, e.g., 0.25 M, may be used in combination with a low pH (∼3.6) to obtain a denser structure. On the other hand, a higher concentration of the buffer with a higher pH (∼5) may be used to obtain the mechanically stable porous membranes. Such control over the precipitation kinetics and the resultant fiber morphology makes the hollow fiber spinning via APS at par with the traditional NIPS.

4. CONCLUSIONS

For the first time, we have successfully demonstrated the production of the hollow fiber membranes via the aqueous phase separation approach. A 35 wt % polymer solution comprising PSS and PEI was prepared by directly mixing the two PE in a monomer molar mixing ratio of 1:2. The high pH dope solution was pushed through a single-orifice spinneret and precipitated under mildly acidic conditions of pH 4 using the acetate buffer as the coagulation bath. A range of suitable hollow fiber spinning conditions for the complexation-based APS has been identified resulting in the formation of the PSS−PEI membranes with tunable membrane morphology. The composition of the bore fluid played a critical role in determining the rate of precipitation, as well as the final structure and properties of the membranes. It was found that having a dense outer skin layer and a relatively porous inner layer is beneficial for obtaining the mechanically stronger hollow fiber membranes. To achieve this result, a well-balanced combination of pH 4 acetate buffer and glycerol solution was used as the bore liquid. Here, the acetate buffer acts as a non-solvent for PSS−PEI, and the added glycerol increases the bore solution viscosity; their appropriate combination produced fibers with good structural integrity. Similarly, the coagulation bath composition is vital for the preparation of these hollow fiber membranes. At low acetate buffer concentrations, such as 0.1 and 0.25 M, the resultant fibers lacked the mechanical strength to withstand water pressures. The membranes prepared in 0.4 M acetate buffer had a pure water permeability of ∼800 $L{\cdot}m^{-2}{\cdot}h^{-1}{\cdot}bar^{-1}$ with 100% oil-droplet retention, making them applicable as microfiltration-type membranes. On the other hand, the membranes prepared in 0.5 and 0.75 M acetate buffer had pure water permeability values of ∼15 and 12 $L{\cdot}m^{-2}{\cdot}h^{-1}{\cdot}bar^{-1}$, respectively, and they were also able to retain 100% of BSA with MWCO in the range of ∼7800−11,600 Da, hence ideal for tight ultrafiltration applications. In addition, the pH of the coagulation bath directly affects the degree of ionization of PEI. At higher pH values such as pH 4.5 and pH 5, PEI is not expected to be fully charged, thereby resulting in less ionic crosslinks and slower precipitation rates, thereby leading to membranes that possess more open and porous lumen structures. The pure water permeabilities of these membranes were ∼60 and ∼260 $L{\cdot}m^{-2}{\cdot}h^{-1}{\cdot}bar^{-1}$ with 100% oil-droplet retentions. In this work, the APS technique is taken one step closer to large-scale production by demonstrating the successful preparation of hollow fiber membranes and broad opportunities to tune the membrane morphology and performance simply by varying the precipitation conditions. The findings of this work can contribute toward the development of a plethora of hollow fiber APS membranes utilizing other polyelectrolyte pairs.

■ ASSOCIATED CONTENT

Supporting Information

The Supporting Information is available free of charge at https://pubs.acs.org/doi/10.1021/acsapm.1c01464.

Experimental setup for determining the pure water permeability and retentions; cross-section and surface SEM images of the hollow fiber membranes prepared at different bore fluid and coagulation bath conditions; sieving curves to determine the molecular weight cut-off of the hollow fiber membranes; long term pure water permeability data with SEM images; AFM and water contact angle.(PDF)

■ AUTHOR INFORMATION

Corresponding Author

Wiebe M. de Vos − *Faculty of Science and Technology, Membrane Science and Technology, MESA+ Institute for Nanotechnology, University of Twente, Enschede 7500 AE, The Netherlands;* orcid.org/0000-0002-0133-1931; Email: w.m.devos@utwente.nl

Authors

Muhammad Irshad Baig − *Faculty of Science and Technology, Membrane Science and Technology, MESA+ Institute for Nanotechnology, University of Twente, Enschede 7500 AE, The Netherlands;* orcid.org/0000-0002-7636-0630

Mehdi Pejman − *Faculty of Science and Technology, Membrane Science and Technology, MESA+ Institute for Nanotechnology, University of Twente, Enschede 7500 AE, The Netherlands; Department of Environment, Land and Infrastructure Engineering (DIATI), Politecnico di Torino, Turin 10129, Italy*

Joshua D. Willott − *Faculty of Science and Technology, Membrane Science and Technology, MESA+ Institute for Nanotechnology, University of Twente, Enschede 7500 AE, The Netherlands;* orcid.org/0000-0003-1870-755X

Alberto Tiraferri − *Department of Environment, Land and Infrastructure Engineering (DIATI), Politecnico di Torino, Turin 10129, Italy;* orcid.org/0000-0001-9859-1328

Complete contact information is available at: https://pubs.acs.org/10.1021/acsapm.1c01464

Notes

The authors declare no competing financial interest.

https://doi.org/10.1021/acsapm.1c01464
ACS Appl. Polym. Mater. XXXX, XXX, XXX−XXX

■ ACKNOWLEDGMENTS

This work was supported by the European Research Council (ERC) under the European Union's Horizon 2020 research and innovation program (ERC StG 714744 SAMBA). We thank Bob Siemerink for his help with building the hollow fiber membrane spinning setup and Xiaoliu Wen for her help with the graphics design.

■ REFERENCES

(1) Baker, R. W. *Membrane Technology and Applications*; 3rd Ed. John Wiley & Sons: Chichester, UK, 2012.
(2) Wu, H.; Shi, C.; Zhu, Q.; Li, Y.; Xu, Z.; Wei, C.; Chen, D.; Huang, X. Capillary-Driven Blood Separation and in-Situ Electrochemical Detection Based on 3D Conductive Gradient Hollow Fiber Membrane. *Biosens. Bioelectron.* **2021**, *171*, 112722.
(3) Wu, H.; Ma, Z.; Wei, C.; Jiang, M.; Hong, X.; Li, Y.; Chen, D.; Huang, X. Three-Dimensional Microporous Hollow Fiber Membrane Microfluidic Device Integrated with Selective Separation and Capillary Self-Driven for Point-of-Care Testing. *Anal. Chem.* **2020**, *92*, 6358−6365.
(4) Razmjou, A.; Resosudarmo, A.; Holmes, R. L.; Li, H.; Mansouri, J.; Chen, V. The Effect of Modified TiO_2 Nanoparticles on the Polyethersulfone Ultrafiltration Hollow Fiber Membranes. *Desalination* **2012**, *287*, 271−280.
(5) Otitoju, T. A.; Ahmad, A. L.; Ooi, B. S. Polyethersulfone Composite Hollow-Fiber Membrane Prepared by in-Situ Growth of Silica with Highly Improved Oily Wastewater Separation Performance. *J. Polym. Res.* **2017**, *24*, 123.
(6) Ong, C. S.; Lau, W. J.; Goh, P. S.; Ng, B. C.; Ismail, A. F. Preparation and Characterization of PVDF−PVP−TiO_2 Composite Hollow Fiber Membranes for Oily Wastewater Treatment Using Submerged Membrane System. *Desalin. Water Treat.* **2015**, *53*, 1213−1223.
(7) Otitoju, T. A.; Ooi, B. S.; Ahmad, A. L. Synthesis of 3-Aminopropyltriethoxysilane-Silica Modified Polyethersulfone Hollow Fiber Membrane for Oil-in-Water Emulsion Separation. *React. Funct. Polym.* **2019**, *136*, 107−121.
(8) Etxeberria-Benavides, M.; Johnson, T.; Cao, S.; Zornoza, B.; Coronas, J.; Sanchez-Lainez, J.; Sabetghadam, A.; Liu, X.; Andres-Garcia, E.; Kapteijn, F.; Gascon, J.; David, O. PBI Mixed Matrix Hollow Fiber Membrane: Influence of ZIF-8 Filler over H_2/CO_2 Separation Performance at High Temperature and Pressure. *Sep. Purif. Technol.* **2020**, *237*, 116347.
(9) Qiu, W.; Vaughn, J.; Liu, G.; Xu, L.; Brayden, M.; Martinez, M.; Fitzgibbons, T.; Wenz, G.; Koros, W. J. Hyperaging Tuning of a Carbon Molecular-Sieve Hollow Fiber Membrane with Extraordinary Gas-Separation Performance and Stability. *Angew. Chemie Int. Ed.* **2019**, *58*, 11700−11703.
(10) Moch, I., Jr. Membranes, Hollow-Fiber. *Kirk-Othmer Encycl. Chem. Technol.* June 17, 2005, *16*, 3, DOI: 10.1002/0471238961.0815121213150308.a01.pub2.
(11) Loeb, S.; Sourirajan, S. Sea Water Demineralization by Means of an Osmotic Membrane. In *Saline Water Conversion—II*; Advances in Chemistry; American Chemical Society: 1963, *38*, 117−132 SE − 38, DOI: 10.1021/ba-1963-0038.ch009.
(12) Reuvers, A. J.; Smolders, C. A. Formation of Membranes by Means of Immersion Precipitation: Part II. the Mechanism of Formation of Membranes Prepared from the System Cellulose Acetate-Acetone-Water. *J. Memb. Sci.* **1987**, *34*, 67−86.
(13) Ulbricht, M. Advanced Functional Polymer Membranes. *Polymer* **2006**, *47*, 2217−2262.
(14) Strathmann, H.; Kock, K. The Formation Mechanism of Phase Inversion Membranes. *Desalination* **1977**, *21*, 241−255.
(15) The European Commission *COMMISSION REGULATION (EU) 2018/ 588 - of 18 April 2018 - Amending Annex XVII to Regulation (EC) No 1907 / 2006 of the European Parliament and of the Council Concerning the Registration, Evaluation, Authorisation and Restr*; Off. J. Eur. Union: 2018, *99*, 3.
(16) Philipp, B.; Dautzenberg, H.; Linow, K. J.; Kötz, J.; Dawydoff, W. Polyelectrolyte Complexes - Recent Developments and Open Problems. *Prog. Polym. Sci.* **1989**, *14*, 91−172.
(17) Fu, J.; Fares, H. M.; Schlenoff, J. B. Ion-Pairing Strength in Polyelectrolyte Complexes. *Macromolecules* **2017**, *50*, 1066−1074.
(18) Schaaf, P.; Schlenoff, J. B. Saloplastics: Processing Compact Polyelectrolyte Complexes. *Adv. Mater.* **2015**, *27*, 2420−2432.
(19) Lankalapalli, S.; Kolapalli, V. R. M. Polyelectrolyte Complexes: A Review of Their Applicability in Drug Delivery Technology. *Indian J. Pharm. Sci.* **2009**, *71*, 481−487.
(20) Decher, G.; Hong, J.-D. Buildup of Ultrathin Multilayer Films by a Self-assembly Process, 1 Consecutive Adsorption of Anionic and Cationic Bipolar Amphiphiles on Charged Surfaces. *Makromol. Chemie. Macromol. Symp.* **1991**, *46*, 321−327.
(21) Tieke, B.; Van Ackern, F.; Krasemann, L.; Toutianoush, A. Ultrathin Self-Assembled Polyelectrolyte Multilayer Membranes. *Eur. Phys. J. E: Soft Matter Biol. Phys.* **2001**, *5*, 29−39.
(22) Malaisamy, R.; Bruening, M. L. High-Flux Nanofiltration Membranes Prepared by Adsorption of Multilayer Polyelectrolyte Membranes on Polymeric Supports. *Langmuir* **2005**, *21*, 10587−10592.
(23) Dubas, S. T.; Farhat, T. R.; Schlenoff, J. B. Multiple Membranes from "True" Polyelectrolyte Multilayers. *J. Am. Chem. Soc.* **2001**, *123*, 5368−5369.
(24) Bruening, M. L.; Dotzauer, D. M.; Jain, P.; Ouyang, L.; Baker, G. L. Creation of Functional Membranes Using Polyelectrolyte Multilayers and Polymer Brushes. *Langmuir* **2008**, *24*, 7663−7673.
(25) Baig, M. I.; Durmaz, E. N.; Willott, J. D.; de Vos, W. M. Sustainable Membrane Production through Polyelectrolyte Complexation Induced Aqueous Phase Separation. *Adv. Funct. Mater.* **2020**, *30*, 1907344.
(26) Durmaz, E. N.; Irshad Baig, M.; Willott, J. D.; de Vos, W. M. Polyelectrolyte Complex Membranes via Salinity Change Induced Aqueous Phase Separation. *ACS Appl. Polym. Mater.* **2020**, *2*, 2612−2621.
(27) Nielen, W. M.; Willott, J. D.; de Vos, W. M. Aqueous Phase Separation of Responsive Copolymers for Sustainable and Mechanically Stable Membranes. *ACS Appl. Polym. Mater.* **2020**, *2*, 1702−1710.
(28) Willott, J. D.; Nielen, W. M.; de Vos, W. M. Stimuli-Responsive Membranes through Sustainable Aqueous Phase Separation. *ACS Appl. Polym. Mater.* **2020**, *2*, 659−667.
(29) Baig, M. I.; Sari, P. P. I.; Li, J.; Willott, J. D.; de Vos, W. M. Sustainable Aqueous Phase Separation Membranes Prepared through Mild PH Shift Induced Polyelectrolyte Complexation of PSS and PEI. *J. Memb. Sci.* **2021**, *625*, 119114.
(30) Baig, M. I.; Willott, J. D.; de Vos, W. M. Tuning the Structure and Performance of Polyelectrolyte Complexation Based Aqueous Phase Separation Membranes. *J. Membr. Sci.* **2020**, *615*, 118502.
(31) Lin, Z.; Chang, J.; Zhang, J.; Jiang, C.; Wu, J.; Zhu, C. A Work-Function Tunable Polyelectrolyte Complex (PEI:PSS) as a Cathode Interfacial Layer for Inverted Organic Solar Cells. *J. Mater. Chem. A* **2014**, *2*, 7788−7794.
(32) Gai, M.; Frueh, J.; Kudryavtseva, V. L.; Mao, R.; Kiryukhin, M. V.; Sukhorukov, G. B. Patterned Microstructure Fabrication: Polyelectrolyte Complexes vs Polyelectrolyte Multilayers. *Sci. Rep.* **2016**, *6*, 1.
(33) Liu, G.; Dotzauer, D. M.; Bruening, M. L. Ion-Exchange Membranes Prepared Using Layer-by-Layer Polyelectrolyte Deposition. *J. Membr. Sci.* **2010**, *354*, 198−205.
(34) Abdu, S.; Martí-Calatayud, M.-C.; Wong, J. E.; García-Gabaldón, M.; Wessling, M. Layer-by-Layer Modification of Cation Exchange Membranes Controls Ion Selectivity and Water Splitting. *ACS Appl. Mater. Interfaces* **2014**, *6*, 1843−1854.
(35) Emonds, S.; Kamp, J.; Borowec, J.; Roth, H.; Wessling, M. Polyelectrolyte Complex Tubular Membranes via a Salt Dilution Induced Phase Inversion Process. *Adv. Eng. Mater.* **2021**, *23*, 2001401.

https://doi.org/10.1021/acsapm.1c01464
ACS Appl. Polym. Mater. XXXX, XXX, XXX−XXX

(36) Tong, W.; Gao, C.; Möhwald, H. Manipulating the Properties of Polyelectrolyte Microcapsules by Glutaraldehyde Cross-Linking. *Chem. Mater.* **2005**, *17*, 4610−4616.
(37) Dickhout, J. M.; Kleijn, J. M.; Lammertink, R. G. H.; De Vos, W. M. Adhesion of Emulsified Oil Droplets to Hydrophilic and Hydrophobic Surfaces-Effect of Surfactant Charge, Surfactant Concentration and Ionic Strength. *Soft Matter* **2018**, *14*, 5452−5460.
(38) Noor, N.; Koll, J.; Scharnagl, N.; Abetz, C.; Abetz, V. Hollow Fiber Membranes of Blends of Polyethersulfone and Sulfonated Polymers. *Membranes* **2018**, *8*, 54.
(39) Bonyadi, S.; Chung, T. S.; Krantz, W. B. Investigation of Corrugation Phenomenon in the Inner Contour of Hollow Fibers during the Non-Solvent Induced Phase-Separation Process. *J. Membr. Sci.* **2007**, *299*, 200−210.
(40) Ahmad, A. L.; Otitoju, T. A.; Ooi, B. S. Hollow Fiber (HF) Membrane Fabrication: A Review on the Effects of Solution Spinning Conditions on Morphology and Performance. *J. Ind. Eng. Chem.* **2019**, *70*, 35−50.
(41) Peng, N.; Widjojo, N.; Sukitpaneenit, P.; Teoh, M. M.; Lipscomb, G. G.; Chung, T.-S.; Lai, J.-Y. Evolution of Polymeric Hollow Fibers as Sustainable Technologies: Past, Present, and Future. *Prog. Polym. Sci.* **2012**, *37*, 1401−1424.
(42) Strathmann, H.; Kock, K.; Amar, P.; Baker, R. W. The Formation Mechanism of Asymmetric Membranes. *Desalination* **1975**, *16*, 179−203.
(43) Smolders, C. A.; Reuvers, A. J.; Boom, R. M.; Wienk, I. M. Microstructures in Phase-Inversion Membranes. Part 1. Formation of Macrovoids. *J. Memb. Sci.* **1992**, *73*, 259−275.
(44) Santoso, Y. E.; Chung, T.-S.; Wang, K. Y.; Weber, M. Chapter 5 - The Investigation of Irregular Inner Skin Morphology of Hollow Fiber Membranes at High-Speed Spinning and the Solutions to Overcome It☆. Chung, T.-S.; Feng, Y. B. T.-H. F. M., Eds.; *Hollow Fiber Membranes Fabrication and Applications*; Elsevier: 2021, 105−122.
(45) Boerlage, S. F. E.; Kennedy, M. D.; Dickson, M. R.; El-Hodali, D. E. Y.; Schippers, J. C. The Modified Fouling Index Using Ultrafiltration Membranes (MFI-UF): Characterisation, Filtration Mechanisms and Proposed Reference Membrane. *J. Membr. Sci.* **2002**, *197*, 1−21.
(46) Chen, Y.; Kim, S.; Cohen, Y. Tuning the Hydraulic Permeability and Molecular Weight Cutoff (MWCO) of Surface Nano-Structured Ultrafiltration Membranes. *J. Memb. Sci.* **2021**, *629*, 119180.
(47) Laakso, T.; Kallioinen, M.; Pihlajamäki, A.; Mänttäri, M.; Wong, J.-E. Polyelectrolyte Multilayer Coated Ultrafiltration Membranes for Wood Extract Fractionation. *Sep. Purif. Technol.* **2015**, *156*, 772−779.
(48) Lentsch, S.; Aimar, P.; Orozco, J. L. Separation Albumin−PEG: Transmission of PEG through Ultrafiltration Membranes. *Biotechnol. Bioeng.* **1993**, *41*, 1039−1047.
(49) Howe, K. J.; Clark, M. M. Fouling of Microfiltration and Ultrafiltration Membranes by Natural Waters. *Environ. Sci. Technol.* **2002**, *36*, 3571−3576.
(50) Nghiem, L. D.; Schäfer, A. I.; Elimelech, M. Pharmaceutical Retention Mechanisms by Nanofiltration Membranes. *Environ. Sci. Technol.* **2005**, *39*, 7698−7705.
(51) Von Harpe, A.; Petersen, H.; Li, Y.; Kissel, T. Characterization of Commercially Available and Synthesized Polyethylenimines for Gene Delivery. *J. Controlled Release* **2000**, *69*, 309−322.
(52) Demadis, K. D.; Paspalaki, M.; Theodorou, J. Controlled Release of Bis(Phosphonate) Pharmaceuticals from Cationic Biodegradable Polymeric Matrices. *Ind. Eng. Chem. Res.* **2011**, *50*, 5873−5876.
(53) Guillen, G. R.; Ramon, G. Z.; Kavehpour, H. P.; Kaner, R. B.; Hoek, E. M. V. Direct Microscopic Observation of Membrane Formation by Nonsolvent Induced Phase Separation. *J. Membr. Sci.* **2013**, *431*, 212−220.

https://doi.org/10.1021/acsapm.1c01464
ACS Appl. Polym. Mater. XXXX, XXX, XXX−XXX